CDCC calculations of fusion of ^{6}Li with targets ^{144}Sm and ^{154}Sm: effect of resonance states *

A. Gómez Camacho[1;1)] J. Lubian[2] H. Q. Zhang(张焕乔)[3,4] Shan-Gui Zhou(周善贵)[5,6,7,8]

[1] Departamento de Aceleradores Instituto Nacional de Investigaciones Nucleares, Apartado Postal 18-1027, C.P. 11801, México, D.F.
[2] Instituto de Fisica Universidade Federal Fluminense, Avenida Litoranea s/n, Gragoatá Niterói, Rio de Janeiro 24210-340, Brazil
[3] China Institute of Atomic Energy, Beijing 102413, China
[4] Department of Technical Physics, Beijing University, Beijing 100871, China
[5] CAS Key Laboratory of Frontiers of Theoretical Physics Institute of Theoretical Physics, Chinese Academy of Sciences, Beijing 100190, China
[6] Center of Theoretical Nuclear Physics National Laboratory of Heavy Ion Accelerator, Lanzhou 730000, China
[7] Synergetic Innovation Center for Quantum Effects and Application Hunan Normal University, Changsha 410081, China
[8] School of Physical Sciences, University of Chinese Academy of Sciences, Beijing 100049, China

Abstract: Continuum Discretized Coupled-Channel (CDCC) model calculations of total, complete and incomplete fusion cross sections for reactions of the weakly bound ^{6}Li with ^{144,154}Sm targets at energies around the Coulomb barrier are presented. In the cluster structure frame of ^{6}Li$\rightarrow\alpha+d$, short-range absorption potentials are considered for the interactions between the ground state of the projectile ^{6}Li and α-d fragments with the target. In order to separately calculate complete and incomplete fusion and to reduce double-counting, the corresponding absorption potentials are chosen to be of different range. Couplings to low-lying excited states 2^{+}, 3^{-} of ^{144}Sm and 2^{+}, 4^{+} of ^{154}Sm are included. So, the effect on total fusion from the excited states of the target is investigated. Similarly, the effect on fusion due to couplings to resonance breakup states of ^{6}Li, namely, $l=2, J^{\pi}=3^{+},2^{+},1^{+}$ is also calculated. The latter effect is determined by using two approaches, (a) by considering only resonance state couplings and (b) by omitting these states from the full discretized energy space. Among other things, it is found that both resonance and non-resonance continuum breakup couplings produce fusion suppression at all the energies considered.

Keywords: weakly bound projectiles, CDCC, total, complete, incomplete fusion

PACS: 24.10Eq, 25.60Pj, 25.60Bx **DOI:** 10.1088/1674-1137/41/12/124103

1 Introduction

Lately, reaction mechanisms involving weakly bound nuclei, both stable and radioactive, have been a focus of experimental and theoretical research [1–5]. Among the most interesting and widely-studied subjects is the effect of breakup of a weakly bound projectile on elastic scattering and fusion reaction processes. The characteristic low binding energy associated with this type of projectile affects reaction mechanisms in two main ways. The first is the static effect due to the large diffusivity of the projectile matter density. This stretched density lowers the Coulomb barrier and hence enhances fusion. The second is that the high projectile breakup probability produces strong repulsive couplings that affect elastic and fusion mechanisms. The repulsive polarization potentials so produced are most important at energies around the barrier and cause fusion suppression.

Other features of reactions with weakly bound nuclei, of current interest, are the different fusion mechanisms that take place, such as complete and incomplete fusion. Complete fusion (CF) can be direct (DCF) or sequential fusion (SCF). Direct complete fusion is a process similar to fusion between strongly bound nuclei, that is, fusion that occurs without a prior excitation of breakup channels. Sequential complete fusion consists of fusion of all the projectile fragments after a previous breakup. From an experimental point of view, it is very difficult to distinguish the evaporation products from a compound nucleus produced by DCF or SCF. Another important reaction mechanism is incomplete fusion (ICF), which is the partial absorption of some fragments while others fly away to the continuum. Total fusion (TF), commonly the quantity measured, is the sum of complete

Received 20 July 2017, Revised 15 September 2017

∗ A. Gómez Camacho from CONACYT, México, J. Lubian from CNPq, FAPERJ, Pronex, Brazil. S.G.Z was partly supported by the NSF of China (11120101005, 11275248, 11525524, 11621131001, 11647601, 11711540016), 973 Program of China (2013CB834400) and the Key Research Program of Frontier Sciences of CAS. H.Q.Z. from NSF China (11375266)

1) E-mail: arturo.gomez@inin.gob.mx

and incomplete fusion. Recently, separate experimental determination of complete and incomplete fusion has been achieved for some reactions with light weakly bound projectiles on medium mass and heavy targets. This has been possible since, different from the case of light targets, compound nuclei decay by the emission of uncharged particles [6–11].

Another important process with weakly bound projectiles that has been extensively studied is the elastic breakup (EB). This mechanism occurs when none of the fragments after breakup is captured by the target. It is now well known that couplings to continuum breakup states have a profound effect on other processes like elastic, inelastic, transfer or fusion reaction mechanisms. To study these effects, a complete theoretical description should include all of the aforementioned reaction channels in a single calculation. Presently, the most powerful theoretical tool to do this type of calculations is the Continuum Discretized Coupled-Channel (CDCC) model [12–14]. This approach has been used in a large range of weakly bound nuclear systems, for instance, a $2n$-halo ^{6}He projectile on ^{59}Co and ^{208}Pb [15, 16], ^{6}Li with targets ^{28}Si, ^{59}Co, ^{58}Ni, ^{144}Sm and ^{208}Pb [12, 15, 17–22], ^{7}Li with ^{28}Si [23, 24] and ^{144}Sm [25], n-halo ^{11}Be with ^{208}Pb [26], and p-halo ^{8}B with ^{58}Ni [19, 27], ^{12}C [28] and ^{208}Pb [29].

Due to the experimental difficulty of performing separate measurements of complete and incomplete fusion cross sections, most of these works study the effect of breakup couplings on elastic scattering or total fusion processes. However, measurements of CF and ICF have recently been reported for some weakly bound nuclei with spherical and deformed medium mass targets. For instance, ^{6}Li with targets ^{96}Zr [30], ^{144}Sm and ^{152}Sm [31, 32], and the projectile ^{9}Be with ^{181}Ta [33], ^{169}Tm and ^{187}Re [34].

Also, measurements of CF and ICF cross sections for the weakly bound ^{6}Li projectile with the highly deformed target ^{154}Sm at energies above the barrier have recently been reported [35]. Here, coupled-channel (CC) calculations are used to study the effect on complete fusion from couplings from inelastic excited states of ^{154}Sm. As expected, this effect is increasingly important as the energy decreases towards the barrier. A comparison of these results with those for the spherical ^{144}Sm is also discussed. Similar, theoretical studies that account for the effect of breakup on complete fusion have been performed for a number of systems, see Refs. [36–38].

Although most of the theoretical efforts are based on slightly modified versions of the CDCC model, which is widely used to manage the effect of breakup states in the continuum on fusion, a considerable theoretical effort has been dedicated to formulate a classical and quantum mechanical treatment of separate ICF and CF cross sections for reactions with weakly bound systems [39–43]. In particular, the classical dynamical model (CDM), described in Refs. [44–47], unambiguously calculates complete and incomplete contributions to total fusion. It is shown in this treatment that the sequential complete fusion process has a more important role in complete fusion than has been assumed. However, the CDM, being a classical model, can calculate fusion at energies above the Coulomb barrier. Tunneling effects at energies below the barrier can be accounted for by a quantum dynamical model like the CDCC. Our calculations of total and incomplete fusion include some energies below the barriers for ^{6}Li+^{144}Sm and ^{6}Li+^{154}Sm. It is interesting to notice that CDM calculations for the system ^{6}Li+^{209}Bi [48] show that the contribution to ICF from α-capture is smaller than that from the deuteron. As will be seen, our calculations show that the contributions to ICF are very similar. Our explanation for this is that while the Coulomb barrier for α+target system is indeed about twice that for deuteron+target, this is compensated by the incident energy E of ^{6}Li being shared by $(2/6)E$ for the deuteron and $(4/6)E$ by the alpha-particle.

In the work presented here, CDCC calculations for total, complete and incomplete fusion cross sections of the weakly bound ^{6}Li projectile with targets ^{144,154}Sm at energies below and above the barrier are performed. In the calculations, we assume the cluster structure of $^{6}\text{Li}\rightarrow \alpha+d$ ($E_{thres} = -1.47$ MeV). Since the masses of the fragments α and d are not so different, their center of mass is not strongly directed towards either of them. Therefore, total fusion cannot be calculated by the absorption of their center of mass as in other weakly bound nuclei, such as the projectile $^{11}\text{Be}\rightarrow{}^{10}\text{Be}+\text{n}$, for which the absorption of the center of mass of ^{11}Be ensures the capture of the charged core ^{10}Be [39]. Hence, total fusion is calculated following the approach given in Ref. [49]. That is, two short-range imaginary potentials inside the $l=0$ nominal Coulomb barrier are used to account for absorption of both or any of the fragments α and d by the target. So, complete and incomplete fusion are implicitly accounted for in this way. These imaginary potentials depend on the relative distance between the fragments and the target. In the coupled-channel equations, we include the lowest excited states of the targets, so as to determine their effect on fusion. The results show that couplings to excited states of the spherical ^{144}Sm and the largely deformed ^{154}Sm produce an increasing total fusion enhancement as the collision energy decreases below the barrier. As will be shown, this effect is more evident for ^{154}Sm than for ^{144}Sm. This indicates that, the strength of the attractive polarization potentials produced by these couplings is stronger for rotational deformed states.

To describe complete and incomplete fusion, we fol-

low the CDCC procedure of V.V. Parkar et al. [50] for the systems ^{6}Li, ^{7}Li with targets ^{209}Bi and ^{198}Pt. That is, real nuclear potentials $V_{\alpha T}$ and V_{dT}, as well as volume Woods-Saxon short-range imaginary potentials $W_{\alpha-T}$ and W_{d-T}, are used for the interactions between the fragments and the target. These potentials depend on the relative coordinates between the projectile fragments and the target. Besides, another short-range imaginary potential W_{P-T} (without a real part) in the incident ^{6}Li(g.s.)-T channel is introduced. The potential W_{P-T} simulates complete fusion between the incident ^{6}Li (g.s.) and the target. Incomplete fusion from deuteron absorption $\sigma_{ICF,d}$ is determined by turning off the imaginary potential W_{d-T}. That is, all fusion absorption $\sigma_{P-T,\alpha}$ come from the W_{P-T} and $W_{\alpha-T}$ potentials. Since total fusion σ_{TF} is previously and separately calculated following Ref. [49], the incomplete fusion from deuteron absorption can be found by $\sigma_{ICF,d}=\sigma_{TF}-\sigma_{P-T,\alpha}$. The parameters of the Woods-Saxon W_{P-T} are fixed so that a CC calculation (without breakup states) fits the complete fusion data of ^{6}Li (g.s.) and the target. Conversely, by turning off the absorption potential between the α-particle and the target $W_{\alpha-T}$, the incomplete fusion $\sigma_{ICF,\alpha}$ can be similarly calculated. Then, complete fusion can be unambiguously determined by $\sigma_{CF}=\sigma_{TF}-\sigma_{ICF,\alpha}-\sigma_{ICF,d}$. It is important to point out that, in the calculation of $\sigma_{ICF,\alpha}$ or $\sigma_{ICF,d}$, absorption by the W_{P-T} potential is considered only for the incident ground state of ^{6}Li. In this way, excited breakup states of ^{6}Li, in which the center of mass of the fragments α–d is inside the range of absorption of W_{P-T}, are excluded. To reduce the possibility of double counting, the range of the potentials $W_{\alpha-T}$ and W_{d-T} will be assumed to be smaller than that of W_{P-T}. This will be explained in more detail in Section 3.

It is important to emphasize that the present calculations assume that the main breakup channel of ^{6}Li is into α and d fragments. It has recently been established [51], however, that significant breakup of ^{6}Li is triggered by neutron (deuteron) transfer forming ^{5}Li(^{8}Be), leading to sequential breakup into α+p (α+α) breakup. However, inclusion of these sequential breakup channels triggered by particle transfer requires more complicated four-body CDCC calculations. Due to the complexity of the numerical calculations these channels have not been considered here.

In a different calculation, the effect of continuum resonance state couplings of the weakly bound nucleus ^{6}Li on total fusion is also studied. We follow a similar technique as in Refs. [52, 53], where the effect on elastic scattering from couplings to resonance continuum states of ^{6}Li was determined for reactions with targets ^{28}Si, ^{58}Ni and ^{144}Sm. It was found that resonant states have an important effect on elastic scattering at the lowest collision energies and for the lightest targets. Following a similar technique, the effect of continuum resonance states l=2, $j^{\pi}=3^{+},2^{+}$, 1^{+} of ^{6}Li on total fusion is studied in this work. Two approaches are used: i) omission of resonant state couplings from the full discretized breakup energy space and ii) considering only the resonance state couplings in the CDCC calculation of fusion, that is, non-resonance states are omitted.

In Section 2, a brief description of the CDCC model is given. Section 3 gives a detailed description of the CDCC discretized energy space for resonance and non-resonance states. A full description of the calculations of total, complete and incomplete fusion cross sections are also given. The results on the effects on fusion from inelastic excited states of the target and from resonance and non-resonance continuum breakup couplings of the projectile are given as well. Finally, a summary and conclusions are presented in Section 4.

2 Brief description of CDCC

A complete description of the CDCC method is given in Refs. [12–14]. Here, only the basic equations that are required to perform our calculations are presented. We consider the two-body cluster structure of ^{6}Li (α-d) with ground state energy $E_{thres}=-1.47$ MeV. The model space for the ground and continuum states of ^{6}Li is that given in Ref. [49]. The wave function for the breakup continuum states of ^{6}Li is

$$\psi^{P}_{lj}(\boldsymbol{r},k)=\{Y_{lm_l}(\hat{\boldsymbol{r}})\otimes\chi_{I\mu s\sigma}\}_{lj}\frac{\varphi_{lsj}(r,k)}{r}, \qquad (1)$$

where the internal wave function of the α-d system is $\chi_{I\mu s\sigma}$, with $I=0$ and $s=1$. $\varphi_{lsj}(r,k)$ describes the α-d relative radial motion with asymptotic wave-number k, orbital angular momentum l and total angular momentum j.

The radial continuum states $\varphi_{lsj}(r,k)$ in Eq. (1) are not square-integrable. However, Ref. [12] provides a prescription for constructing square-integrable wave functions known as bin states. A bin state $u^{(i)}_{\beta}(r)$ is obtained by a superposition of scattering wave functions within a given interval i, of continuum k values, $k_{i-1}<k<k_i$, i.e.,

$$u^{(i)}_{\beta=lsj}(r)=\sqrt{\frac{2}{\pi\eta_l}}\int_{k_{i-1}}^{k_i} w_i(k,l)\mathrm{e}^{-\mathrm{i}\delta_k(l)}\varphi_{lsj}(r,k)\mathrm{d}k, \qquad (2)$$

where $\delta_k(l)$ are scattering phase-shifts of φ_{β} and $w_i(k,l)$ are weight functions defined by,

$$\eta_l=\int_{k_{i-1}}^{k_i}|w_i(k,l)|^2\mathrm{d}k. \qquad (3)$$

Actually, the weight functions w_i associated with non-resonant bin states are usually set as $w_i(k,l)=1$, while for resonant states $w_i(k,l)=\sin[\delta_k(l)]$.

The total wave function of the three-body system (α-*d-target*) is given by,

$$\Psi(\boldsymbol{R},\boldsymbol{r},\xi)=\sum_q\sum_\beta F_{\beta q}(\boldsymbol{R})\psi^P_\beta(\boldsymbol{r})\otimes\Phi^T_q(\xi), \qquad (4)$$

where $\Phi^T_q(\xi)$, q = 0,1,2,3.. correspond to the ground and inelastic states of the target satisfying $H^T\Phi^T_q(\xi)=\varepsilon^T_q\Phi^T_q(\xi)$. $F_{\beta q}(\boldsymbol{R})$ represents the projectile-target relative motion in the βq-channel. Projecting the equation of motion of the system onto the projectile states β and onto the excited states of the target q, the following coupled equations are obtained,

$$\left[\hat{T}_R+U^{(J)}_{\beta q,\beta q}(R)-(E-\varepsilon_\beta-\varepsilon^T_q)\right]F^{(J)}_{\beta q}(R)=$$
$$-\sum_{\beta' q'}U^{(J)}_{\beta q,\beta' q'}(R)F^{(J)}_{\beta' q'}(R). \qquad (5)$$

Here, ε_β is the excitation energy of the projectile in the β-state. $U^{(J)}_{\beta q,\beta q}$ and $U^{(J)}_{\beta q,\beta' q'}$ are the radial dependent diagonal and non-diagonal matrices of the interaction potentials $\hat{V}_{dT}+\hat{V}_{\alpha T}$, where $\hat{V}_{dT}$ and $\hat{V}_{\alpha T}$ are the nuclear interactions between the deuteron and α-particle with the target. Notice that $U^{(J)}_{00,00}$ corresponds to the elastic incident channel. As a matter of fact, the interaction potential matrices are given by,

$$U^{(J)}_{\beta q\beta' q'}(R)=<u_\beta\Phi^T_q\left|\hat{V}_{dT}(\boldsymbol{r}_{dT},\xi)+\hat{V}_{\alpha T}(\boldsymbol{r}_{\alpha T},\xi)\right|u_{\beta'}\Phi^T_{q'}>, \qquad (6)$$

where $\boldsymbol{r}_{dT}=\boldsymbol{R}-\frac{2}{6}\boldsymbol{r}$ and $\boldsymbol{r}_{\alpha T}=\boldsymbol{R}+\frac{4}{6}\boldsymbol{r}$ represent the radial distance between the fragments and the target. The integrations in Eq. (6) are carried out over the internal radial coordinate $\boldsymbol{r}$, the angular coordinates of $\boldsymbol{R}$ and the internal coordinates of the target ξ.

The code FRESCO [54] will be used in our calculations of fusion. It is important to mention the approximations we adopted, to account for the collective degrees of freedom of the target in conjunction with breakup states of the projectile. First, inelastic states of the projectile are not considered. Now, in the coupling matrix elements $U^J_{\beta=0,\beta'=0}(R)$, the single folding of the interaction potentials over the projectile g.s. wave function, i.e., $<u_0|\hat{V}_{dT}+\hat{V}_{\alpha T}|u_0>$, is calculated and expanded in multipoles as in the usual coupled channel calculations. On the other hand, to introduce simultaneous target excitation and projectile continuum, multipole expansion of the $\alpha-$target and deuteron-target potentials is carried out. These potentials depend not only on their relative distance, but also on the internal degrees of freedom of the target. Then Eq. (6) is integrated over all the variables except the fragment-target relative distance. The procedure of decoupling target excitations and breakup states of the projectile is shown in detail in Ref. [55], where applications to some reactions with weakly bound projectiles are presented as well. In particular, we used CDCC to calculate the ground state optical potential by folding the $\alpha-$target and deuteron-target potentials by the ground state of the projectile, considering that the target is in its ground state. This potential was then deformed to account for target excitation. Finally, when one compares the results of Refs. [55] and Ref. [56] for ^{6}Li + ^{144}Sm, a system studied in this work, the results of the full calculation and the decoupling results for the elastic and inelastic excitation of the target are very similar, showing that this approximation might be quite reasonable. For this reason we will adopt this approximate procedure in the present work.

3 Calculations

3.1 Discretization of continuum space and nuclear interaction potentials

The ground and discretized breakup states of ^{6}Li$\rightarrow d$+α are constructed by using the interaction given in Ref. [49]. The discretization of the continuum is made as follows. The maximum angular momentum for the relative motion of the fragments is $l_{\max}$=3. Larger values do not have any effect on the calculated fusion cross sections. Bin states are constructed from an initial energy $\varepsilon_0=0$ MeV (above the threshold energy $E_{\rm thres}=-1.47$ MeV) up to a maximum energy $\varepsilon_{\max}=6.8$ MeV. For states with $l=0$, $j^\pi=1^+$ and $l=1$, $j^\pi=0^-,1^-,2^-$, an energy step is fixed at $\Delta\varepsilon=0.5$ MeV. Finer and variable steps are used for the resonant states l=2, j^π=3$^+$,2$^+$, 1$^+$, so as to obtain centroid excitation energies and widths close to the corresponding measured values [49]. For bin states l=3, j^π=4$^+$,3$^+$,2$^+$, a larger step $\Delta\varepsilon$=1.0 MeV is used. Convergence tests at $\varepsilon_{\max}=7.0$,7.5 and 8.0 MeV were done with no effect on fusion. Similarly, larger steps $\Delta\varepsilon=0.75$ and 1.0 MeV were used with no appreciable effect. Coulomb and nuclear potential multipoles are included up to L_Q=4.

As for the nuclear interactions between the fragments α, d and the target of Eq. (6), we use the same potentials as in our previous work for elastic scattering [52, 53]. That is, the systematic Woods-Saxon potentials of Ref. [57] for $\hat{V}_{dT}$ and the density dependent double-folding Sao Paulo potential (SPP) for $\hat{V}_{\alpha T}$ [58, 59]. These potentials have been modified to account for vibrational and deformed effects of the excited states of the targets. The following excited states are included: for the spherical ^{144}Sm, the 2$^+$ (1160 keV) and 3$^-$ (1810 keV) states with β_2=0.087 and β_3=0.15; for the deformed ^{154}Sm, the 2$^+$ (82 keV) and 4$^+$ (267 keV) states, with deformation parameters β_2=0.34 and β_4=0.08 [60–62].

3.2 Total, complete and incomplete fusion

CDCC elastic scattering angular distributions and the effect of resonances of the projectile ^{6}Li with targets ^{28}Si, ^{58}Ni and ^{144}Sm have been reported in Refs. [52, 53].

In these calculations, the volume and surface imaginary potentials of Refs. [57–59] were used for the $\alpha-T$ and d–T interactions. In the calculations presented here, the deformed nuclear potentials of Refs. [57–59] are used, but short-range volume imaginary potentials are applied to account for fragment-target fusion absorption. The inclusion of an adequate surface Woods-Saxon potential W_S in the elastic incident channel of ^{6}Li-target, in the region of strong absorption, would certainly be more realistic. By fitting the parameters of W_S, the calculated total reaction $\sigma_{TR}=\sigma_{TF}+\sigma_{DR}$, given by

$$\sigma_R=\frac{2}{\hbar v}\sum_{\beta qJ}\frac{1}{2J+1}<F^{(J)}_{\beta q}|W|F^{(J)}_{\beta q}>, \qquad (7)$$

where $W=W_F+W_S$, would become closer to the data and hence elastic scattering. However, the fusion cross section would not be appreciably affected. We have performed calculations with the inclusion of a surface potential with parameters $W_{S0}=10.0$ MeV, $r_{S0}=1.4$ fm and $a_{S0}=0.4$ fm in the elastic channel for ^{144}Sm and ^{144}Sm at some energies below and above the barrier. The results show an effect on fusion around 1% for the higher energies and 8% for the lower energies with respect to when W_S is not included. Thus, in what follows only imaginary short-range potentials are used in the fragment-target interactions.

In the first calculation, the total fusion cross section σ_{TF} between the ^{6}Li projectile and targets ^{144}Sm and ^{154}Sm is determined for incident energies around and above the Coulomb barriers. Two short-range imaginary volume Woods-Saxon potentials $W_{\alpha-T}$ and W_{d-T} are considered to account for absorption of the α-particle and deuteron by the target. Both $W_{\alpha-T}$ and W_{d-T} depend on the radial distance between the fragments and the target respectively. Therefore, when both fragments or any one of them are inside the range of these potentials, complete or incomplete fusion is accounted for. The parameters of these potentials are fixed with strength $W_0=25$ MeV, reduced radius $r_0=0.9$ fm and diffuseness $a_0=0.1$ fm for both ^{144}Sm and ^{154}Sm. Absorption by these potentials happens inside the corresponding Coulomb barriers, $V_{B,d}=13.92$ MeV, $R_{B,d}=6.4$ fm and $V_{B,\alpha}=26.5$ MeV, $R_{B,\alpha}=6.83$ fm, respectively. So, the incident flux that passes above or through the barrier, inside the short-range potential, contributes to fusion. Figure 1(a) shows the results of σ_{TF} for the system ^{6}Li+^{144}Sm. The calculation with the whole energy state spectrum, that is, ground and discrete breakup state couplings of the projectile and inelastic state couplings of the target, is presented by the solid line. The calculation without excited states of the target, that is, when couplings between ground states of the target and projectile are considered, as well as breakup states of the projectile, is shown by the dashed line. The calculation for the elastic channel, i.e., without couplings from continuum breakup states of the projectile and excited states of the target, is shown by the dashed-dotted line. The total fusion data of Fig. 1(a) are obtained by the sum of complete and incomplete fusion data of Refs. [31, 32]. The results show that the calculated total fusion is above the data for energies above the barrier, however there is a better agreement around and below the barrier.

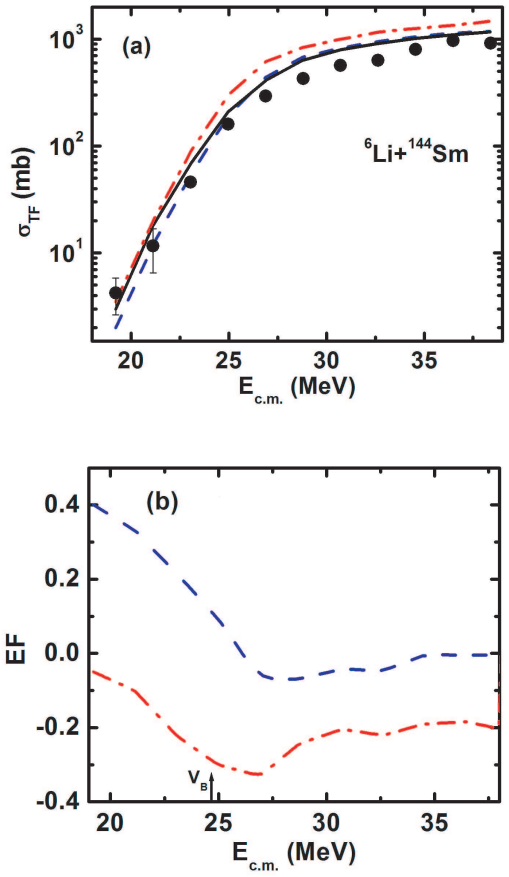

Fig. 1. (color online) (a) Total fusion cross section for ^{6}Li+^{144}Sm with the full breakup space of ^{6}Li (solid line), without excited states of the target (dashed line) and without breakup states of the projectile (dashed-dotted line). (b) Fusion enhancement and suppression factors from excited states of ^{144}Sm (dashed line) and from breakup states of ^{6}Li (dashed-dotted line).

Regarding the sensitivity of the TF calculations just described, with respect to the short-range potential parameters, it is important to point out that smaller values of the reduced radius parameter r_0 do not have an appreciable effect as long as $R=r(A_T^{1/3}+A_{^6Li}^{1/3})$ is well inside the Coulomb barrier. With respect to the strength W_0 and diffuseness a_0, there is no effect if the range of the po-

tential is larger than the mean free path of the fragment inside the barrier [49].

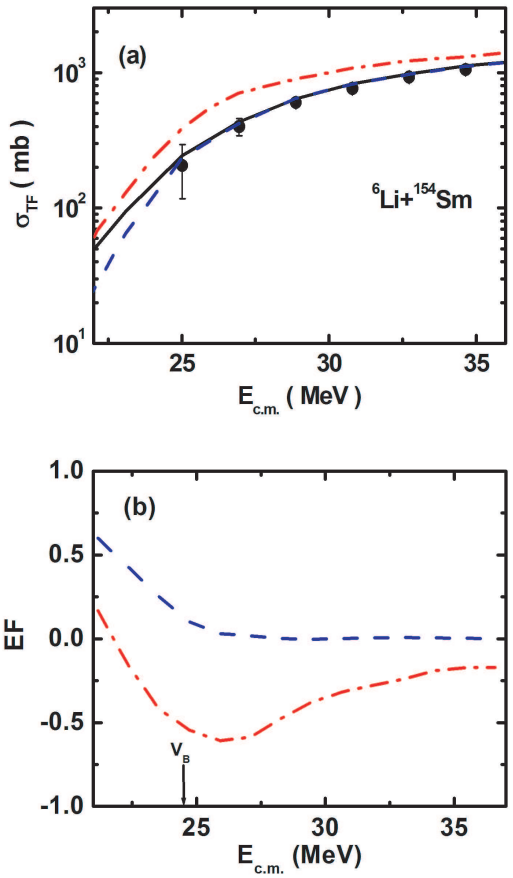

Fig. 2. (color online) (a) Total fusion cross section for ^{6}Li+^{154}Sm with the full breakup space of ^{6}Li (solid line), without excited states of the target (dashed line) and without breakup states of the projectile (dashed-dotted line). (b) Fusion enhancement and suppression factors from excited states of ^{154}Sm (dashed line) and from breakup states of ^{6}Li (dashed-dotted line).

Figure 1(b) shows the numerical effect EF on total fusion due to couplings from inelastic excited states of the target (dashed line) and from continuum breakup states of ^{6}Li (dashed-dotted line). EF is defined by

$$EF=1-\frac{\sigma_{F,n}}{\sigma_{TF}}, \tag{8}$$

where $\sigma_{F,n}$ with $n=1$ is the calculation without couplings from inelastic states of the target and with $n=2$ is that without breakup couplings of the projectile. Couplings to inelastic excited states of ^{144}Sm enhance fusion, particularly for energies around and below the Coulomb barrier. Here, the enhancement factor EF reaches a value of about 38% at $E_{c.m.}=20$ MeV. On the other hand, the effect of couplings to breakup states of the projectile produces a net fusion suppression for all energies. The strength of the suppression factor EF increases as the collision energy decreases towards the barrier V_B to then decrease at lower energies. That is, breakup state couplings produce a net repulsive potential that increases the fusion barrier and therefore reduces fusion. Figure 2 shows the corresponding results for ^{154}Sm. The solid line of Fig. 2(a) presents the total fusion calculation with all couplings, while the circles represent the data of Ref. [35]. The dashed line of Fig. 2(b) shows that the effect of the excited states of the deformed ^{154}Sm is stronger than for the spherical ^{144}Sm at energies below the barrier. The enhancement factor EF reaches a value of about 50% at $E_{c.m.}=22$ MeV, while for ^{144}Sm it is about 30%. The dashed-dotted line of Fig. 2(a) shows that breakup state couplings of the projectile are essential to fit the data. This can be seen in Fig. 2(b), where it is observed that these couplings produce a net repulsive effect that raises the barrier. Breakup state couplings are more important for ^{154}Sm than for ^{144}Sm, as shown by the dotted-dashed lines of Figs. 1(b) and 2(b).

Complete and incomplete fusion cross sections are calculated in a similar manner as in Ref. [50]. That is, besides $W_{\alpha-T}$ and W_{d-T}, another short-range imaginary potential W_{P-T} is included to *simulate* fusion absorption from the ground state incident channel of ^6Li-T. Then, either $W_{\alpha-T}$ or W_{d-T} is turned off and we calculate, say, $\sigma_{P-T,d}$ ($W_{\alpha-T}=0$), that accounts for fusion absorption through the incident and $d-T$ channels. Similarly, if $W_{d-T}=0$, we calculate $\sigma_{P-T,\alpha}$, which is fusion through the incident and $\alpha-T$ channels. It should be noted that W_{P-T} is not generated by $W_{\alpha-T}$ and W_{d-T}, since one of these potentials is set to zero. Then, by using the previous calculation of total fusion σ_{TF}, it is possible to determine the incomplete fusion from deuteron absorption by $\sigma_{ICF,d}=\sigma_{TF}-\sigma_{P-T,\alpha}$. Clearly, $\sigma_{ICF,\alpha}$ can be determined in a similar manner. It is important to indicate that absorption by the potential W_{P-T} is not directly complete fusion absorption, but instead, it is only useful to calculate absorption of any fragment. As a matter of fact, once the total incomplete fusion $\sigma_{ICF}=\sigma_{ICF,\alpha}+\sigma_{ICF,d}$ is known, complete fusion σ_{CF} can be determined by $\sigma_{CF}=\sigma_{TF}-\sigma_{ICF}$. It should also be established that, in the calculation of $\sigma_{P-T,\alpha}$ and $\sigma_{P-T,d}$, double counting occurs only when the center of mass of the ground state of the ^6Li projectile and either one of the fragments are simultaneously inside their corresponding regions of absorption. So, to reduce double counting, the regions of absorption of $W_{\alpha-T}$ and W_{d-T} are assumed to be much shorter than that of W_{P-T}. In the calculations, we fix the parameters as $W_{P-T}=50$ MeV, reduced radius $r_{P-T}=1.0$ fm and diffuseness $a_{P-T}=0.4$ fm for both targets

^{144,154}Sm. For the potentials $W_{\alpha-T}$ and W_{d-T}, the same parameters as Ref. [50] are used. As in the case of total fusion, similar considerations are relevant regarding the sensitivity of the calculations with respect to these parameters. Particularly, the reduced radius $r=0.62$ fm for $\alpha-T$ and $r=0.66$ fm for $d-T$ guarantee that the imaginary potentials are centered well inside the respective Coulomb barriers.

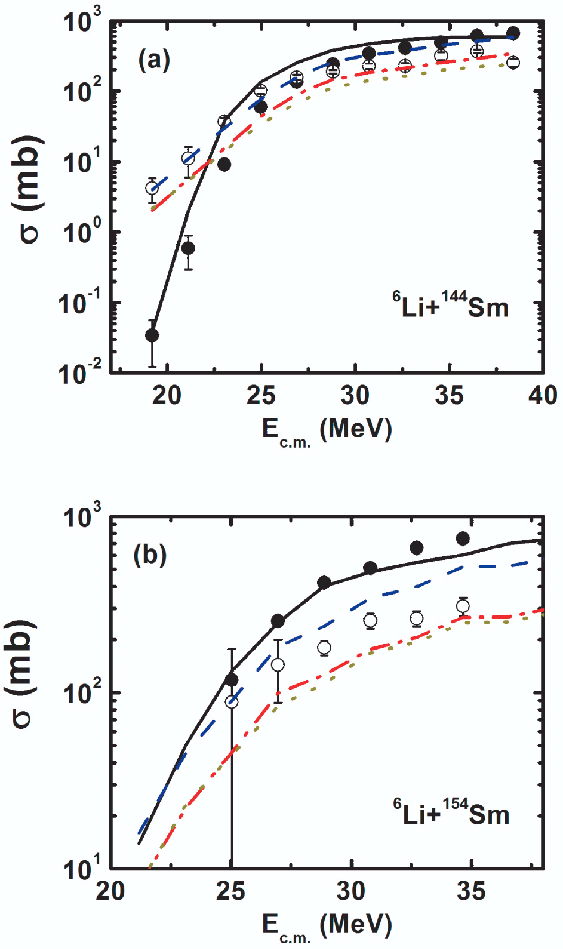

Fig. 3. (color online) (a) Complete (solid line) and incomplete (dashed line) fusion cross sections for the reaction ^{6}Li+ ^{144}Sm. The dashed-dotted line represents the contribution to ICF from α-particle absorption while the dotted line corresponds to deuteron absorption. (b) The same as (a) but for ^{154}Sm.

The potentials are centered about 2 fm inside the barrier. Figures 3(a) and (b) show the results for ^{144}Sm and ^{154}Sm respectively. The experimental data for complete (full circles) and incomplete fusion (empty circles) are those of Refs. [31, 32] for ^{144}Sm and Ref. [35] for ^{154}Sm. The complete fusion calculation (solid lines) is slightly above the data for ^{144}Sm, while there is a better agreement for ^{154}Sm. For both targets, incomplete fusion results (dashed lines) are close to the data at energies around the Coulomb barrier and over-predicted for higher energies. In both cases, incomplete fusion becomes more important than complete fusion at energies below the barriers. Also, incomplete fusion from α-particle absorption (dashed-dotted lines) is rather similar to that of deuteron absorption (dotted lines) except at the higher energies where it is slightly stronger. This result agrees with the calculations of Ref. [50] for the ^{6}Li projectile with ^{209}Bi and ^{198}Pt targets. That is, deuteron and α-particle absorption are of similar magnitude. It is equally important to point out that the independent calculations of incomplete fusion for both fragments neglects the correlation that can appear by the absorption of one fragment on the other. This effect is negligible if breakup of the projectile happens at large distances from the target. The fact that the calculations for complete and incomplete fusion are above the data for ^{144}Sm, as Fig. 3(a) shows, is consistent with the calculation for total fusion of Fig. 1(a), where there is also an over-prediction. Also, from Fig. 3(b) for ^{154}Sm, a better agreement for CF is observed except at the higher energies, where the calculated values are below the data. The ICF results are above the data for the higher energies. Since the calculated total fusion of Fig. 2(a) for ^{154}Sm is in good agreement with the corresponding data at all energies, the effect of double counting can be inferred from the behavior of the CF and ICF results. It is clear that the effect is stronger at higher energies for both CF and ICF. This can be understood as follows: at high collision energies, it is easier for both the incident ground state of the projectile and either one of the fragments to be inside their regions of absorption.

3.3 Effect of resonance and non-resonance breakup states on fusion

In this section, we present the calculations of the effect on total fusion from resonance breakup states $l=2$, $j^\pi = 3^+, 2^+, 1^+$ of the weakly bound nucleus ^{6}Li. The procedure is the same at that used in Refs. [52, 53], where a study of the effect of these resonances on elastic scattering was presented. Two different calculations are performed, First, fusion is calculated when resonance states are excluded from the full discretized energy space, and then when only couplings between the elastic channel and resonance states are considered. The results are shown in Fig. 4(a) for ^{144}Sm and Fig. 4(b) for ^{154}Sm. The solid lines represent the calculation with the full discretized energy space, the dashed lines the case when only couplings between resonance states are included, and the dashed-dotted lines the case when resonance states are omitted from the full space. The effects of

resonance and non-resonance subspace couplings are of similar magnitude for each target but are more important for ^{154}Sm than for ^{144}Sm. Also, for all the energies considered, both calculations are above that for the full discretized space. This implies that separate couplings of resonance and non-resonance subspaces generate net repulsive polarization potentials, that in turn raise the Coulomb barrier and thus suppress fusion. Moreover, the fact that the effect is more evident for ^{154}Sm than for ^{144}Sm implies that the deformed Coulomb and nuclear potentials of Eq. (6) produce stronger repulsive polarizations than for the vibrational ^{144}Sm.

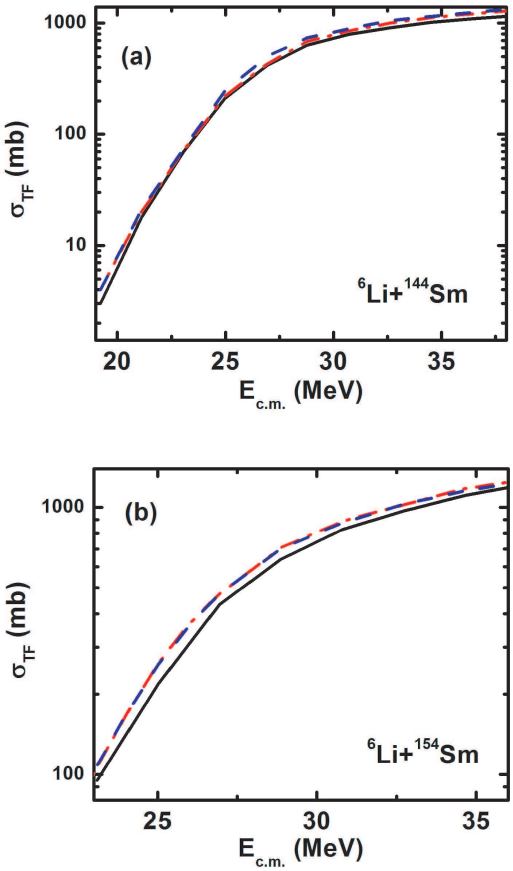

Fig. 4. (color online) (a) Total fusion cross section for ^{144}Sm with the full breakup space of ^{6}Li (solid line), with only couplings from resonance breakup states (dashed line), and with only non-resonance ones (dashed-dotted line). (b) The same as (a) but for ^{154}Sm.

4 Summary and conclusions

CDCC calculations of total, complete and incomplete fusion cross sections have been presented for the nuclear systems ^{6}Li with targets ^{144}Sm and ^{154}Sm at energies around and above the Coulomb barrier. In the CDCC calculations, resonance and non-resonance states of ^{6}Li were discretized up to a maximum energy of 6.8 MeV with discretization steps such that centroid energies of the resonances and widths are close to the experimental values. To account for the effect of excited states of the targets on fusion, low-lying excited states were included in the calculations. The cluster structure of the projectile ^{6}Li$\rightarrow\alpha+d$ was assumed, with global nuclear interactions for the α-target and d-target sub-systems. For the energies around the barrier studied in this work, it has been shown that calculations with coupling to only the elastic channel (without breakup discretized states) are insufficient to fit the fusion data, so couplings to breakup states are very important. On the other hand, the effect of inelastic states of the targets produce attractive polarizations, that in turn, lower the fusion barrier and hence enhance fusion. This effect is larger for the deformed ^{154}Sm than for the spherical ^{144}Sm. For the calculation of total fusion, short-range imaginary fusion potentials inside the Coulomb barrier have been used for absorption of the fragments α and d by the target. So, complete fusion is accounted for when both fragments are inside the region of absorption, and incomplete fusion when only one of them is inside.

To calculate the contributions to incomplete fusion from α-particle or deuteron capture, another imaginary potential for absorption through the incident channel was introduced (^{6}Li in the ground state). Then, fusion absorption in the incident and any one of the fragments was calculated by turning off the imaginary potential of any one of the fragments. The imaginary potential in the incident channel is not generated by those corresponding to the fragments, since one of them is turned off. To reduce double counting, the short range potentials were chosen to have different ranges. The result of this calculation was subtracted from the prior calculation of total fusion to determine the fragment contribution. Therefore, incomplete fusion for α-particle and deuteron was explicitly calculated. Once the total incomplete fusion is known, complete fusion was similarly calculated by subtraction from total fusion.

In a different calculation, the effect on total fusion due to couplings from resonance state couplings of ^{6}Li, namely, $l=2$, $J^\pi=3^+,2^+$ and 1^+, has been presented. This effect was calculated by following two approaches, (a) by omitting the states corresponding to the resonances from the whole energy discrete space and (b) by considering only resonance state couplings. The effects of resonance and non-resonance couplings are stronger for ^{154}Sm than for ^{144}Sm. This is due to the deformed Coulomb and nuclear potentials used for the interactions between the fragments α and d with ^{154}Sm. These deformed potentials produce stronger repulsive polariza-

tion potentials than those for the vibrational ^{144}Sm.

Finally, it is important to mention that, in order to obtain a complete picture of the projectile breakup effect on fusion, couplings of transfer-triggered breakup channels, along with α+d, should be included in the CDCC calculation.

References

1 L. F. Canto, P. R. S. Gomes, R. Donangelo et al, Phys. Rep., **424**: 1 (2004)
2 J. F. Liang, C. Signorini, Int. J. Mod. Phys. E, **14**: 1121 (2005)
3 N. Keeley, R. Raabe, N. Alamanos et al, Prog. Part. Nucl. Sci., **59**: 579 (2007)
4 L.F. Canto, P.R.S. Gomes, R. Donangelo et al, Phys. Rep., **596**: 1 (2015)
5 P. R. S. Gomes, J. Lubian, L. F. Canto et al, Few-body Systems, **57**: 165 (2016)
6 M. Dasgupta, D. J. Hinde, R. D. Butt et al, Phys. Rev. Lett., **82**: 1395 (1999)
7 M. Dasgupta, D. J. Hinde, K. Hagino et al, Phys. Rev. C, **66**: 041602(R) (2002)
8 M. Dasgupta, P. R. S. Gomes, D. J. Hinde et al, Phys. Rev. C, **70**: 024606 (2004)
9 C. Signorini, Z. H. Liu, Z. C. Li et al, Eur. Phys. J. A, **5**: 7 (1999)
10 P. R. S. Gomes, I. Padron, E. Crema et al, Phys. Lett. B, **634**: 356 (2006)
11 P. R. S. Gomes, I. Padron, E. Crema et al, Phys. Rev. C, **73**: 064606 (2006)
12 Y. Sakuragi, M. Yahiro, and M. Kamimura, Prog. Theor. Phys. Suppl., **89**: 1 (1986)
13 Y. Sakuragi, M. Yahiro, and M. Kamimura, Prog. Theor. Phys., **70**: 1047 (1983)
14 N. Austern, Y. Iseri, M. Kamimura et al, Phys. Rep., **154**: 125 (1987)
15 C. Beck , N. Keeley, A. Diaz-Torres, Phys. Rev. C, **75**: 054605 (2007)
16 J. P. Fernandez-Garcia, M. A. G. Alvarez, A. M. Moro et al, Phys. Lett. B, **693**: 310 (2010)
17 K. Zerva, N. Patronis, A. Pakou et al, Phys. Rev. C, **80**: 017601 (2009)
18 K. Rusek, N. Keeley, A. Pakou et al, Nucl. Phys. A, 2007, **784**: 13 (2007)
19 N. Keeley, R. S. Mackintosh, and C. Beck, Nucl. Phys. A, **380**: 1 (2010)
20 N. Keeley and K. Rusek, Phys. Lett. B, **375**: 9 (1996)
21 D. R. Otomar, J. Lubian, and P. R. S. Gomes, Eur. Phys. J. A., **46**: 285 (2010)
22 G. R. Kelly, N. J. Davis, R. P. Ward et al, Phys. Rev. C, **63**: 024601 (2000)
23 A. Pakou, N. Alamanos, G. Gillibert et al, Phys. Rev. C, **69**: 054602 (2004)
24 A. Pakou, K. Rusek, N. Alamanos et al, Eur. Phys. J. A., **39**: 187 (2009)
25 D. R. Otomar, J. Lubian, P. R. S. Gomes et al, Phys. Rev. C, **80**: 034614 (2009)
26 L. F. Canto, J. Lubian, P. R. S. Gomes et al, Phys. Rev. C, **80**: 047601 (2009)
27 J. Lubian, T. Correa, E. F. Aguilera et al, Phys. Rev. C, **79**: 064605 (2009)
28 B. Paes, J. Lubian, P. R. S. Gomes et al, Nucl. Phys. A, **890**: 1 (2012)
29 J. Rangel, J. Lubian, L. F. Canto et al, Phys. Rev. C **93**: 054610 (2016)
30 S. P. Hu, G. L. Zhang, J. C. Yang et al, Phys. Rev. C, **91**: 044619 (2015)
31 P. K. Rath, S. Santra, N. L. Singh et al, Phys. Rev. C, **79**: 051601 (2009)
32 P. K. Rath, S. Santra, N. L. Singh et al, Nucl. Phys. A, **874**: 14 (2012)
33 N. T. Zhang, D. Y. Fang, P. R. S. Gomes et al, Phys. Rev. C, **90**: 024621 (2014)
34 Y. D. Fang, P. R. S. Gomes, J. Lubian et al, Phys. Rev. C, **91**: 014608 (2015)
35 C. L. Guo, G. L. Zhang, S. P. Hu et al, Phys. Rev. C, **92**: 014615 (2015)
36 M. F. Guo, G. L Zhang, P. R. S. Gomes et al, Phys. Rev. C, **94**: 044605 (2016)
37 Bing Wang, Wei-Juan Zhao, P. R. S. Gomes et al, Phys. Rev. C, **90**: 034612 (2014)
38 Bing Wang, Wei-Juan Zhao, A. Diaz-Torres et al, Phys. Rev. C, **93**: 014615 (2016)
39 A. Diaz-Torres and I. J. Thompson, Phys. Rev. C, **65**: 024606 (2002)
40 K. Hagino, A. Vitturi, C. H. Dasso et al, Phys. Rev. C, **61**: 037602 (2000)
41 K. Rusek, N. Alamanos, N. Keeley et al, Phys. Rev. C, **70**: 014603 (2004)
42 H. D. Marta, L. F. Canto, R. Donangelo, Phys. Rev. C, **89**: 034625 (2014)
43 S. Hashimoto, K. Ogata, S. Chiba et al, Prog. of Theor. Phys., **122**: 1291 (2009)
44 Maddalena Boselli and Alexis Diaz-Torres, J. Phys. G, Nucl. Part. Phys., **41**: 094001 (2014)
45 M. Boselli and A. Diaz-Torres, Phys. Rev. C, **92**: 044610 (2015)
46 A. Diaz-Torres, D. J. Hinde, J. A. Tostevin et al, Phys. Rev. Lett., **98**: 152701 (2007)
47 A. Diaz-Torres, J. Phys. G, Nucl. Part. Phys., **37**: 075109 (2010)
48 A. Diaz-Torres, D. Quraishi, unpublished
49 A. Diaz-Torres, I. J. Thompson, and C. Beck, Phys. Rev. C, **68**: 044607 (2003)
50 V. V. Parkar, V. Jha, and S. Kailas, Phys. Rev. C, **94**: 024609 (2016)
51 D. H. Luong, M. Dasgupta, D. J. Hinde et al, Phys. Rev. C, **88**: 034609 (2013)
52 A. Gómez Camacho, A. Diaz-Torres, P. R. S. Gomes et al, Phys. Rev. C, **91**: 014607 (2015)
53 A. Gómez Camacho, A. Diaz-Torres, P. R. S. Gomes, and J. Lubian, Phys. Rev. C, **93**: 024604 (2016)
54 I. J. Thompson, Comput. Phys. Rep., **7**: 167 (1988)
55 M. Gómez-Ramos and A. M. Moro, Phys. Rev. C, **95**: 034609 (2017)
56 A. Woodard, J. Figueira, D. Otomar et al, Nucl. Phys. A, **873**: 17 (2012)
57 H. An and C. Cai, Phys. Rev. C, **73**: 054605 (2006)
58 L. C. Chamon, D. Pereira, M. S. Hussein et al, Phys. Rev. Lett., **79**: 5218 (1997)
59 L. C. Chamon B. V. Carlson, L. R. Gasques et al, Phys. Rev. C, **66**: 014610 (2002)
60 S. Raman, C. W. Nestor Jr, and P. Tikkanem, At. Data Nucl. Data Tables, **78**, 1 (2001)
61 T. Kibedi and R. H. Spear, At. Data Nucl. Data Tables, **80**: 35 (2001)
62 J. R. Leigh, M. Dasgupta, D. J. Hinde et al, Phys. Rev. C, **52**: 3151 (1995)